WWW.IJRPR.COM

International Journal of Research Publication and Reviews

Journal homepage: www.ijrpr.com ISSN 2582-7421

Modeling and Simulation of Data for the Identification and Prediction of the Behavior of Lake Alaotra in Magascar

Rabotovao David Sebas [1], Andriazafimahazo Lahinirina Fridolin [2], Ratsimbazafy Aro Pascal [3], Robijaona Rahelivololoniaina Baholy [4], Rajaonah Rabevala [5]

1. Renewable Energy and Environment Thematic Doctoral School, University of Antsiranana, Antsiranana, Madagascar
2. Faculties of science, Applied Physics Laboratory, University of Fianarantsoa, Fianarantsoa, Madagascar
3. Higher Normal School, Applied Physics Laboratory, University of Fianarantsoa, Fianarantsoa, Madagascar
4. Doctoral School of Industrial Agricultural and Food Process Engineering, University of Antananarivo, Antanarivo, Madagascar
5. Higher Polytechnic School Applied Mechanics Laboratory,University of Antsiranana, Antsiranana, Madagascar
***Email**: sebasdavid4226@gmail.com,*

A B S T R A C T

The sustainable management of the Lake Alaotra-Mangoro system, a vital ecological and socio-economic resource in eastern Madagascar, is severely threatened by rapid anthropogenic pressures and climate change. This study aimed to characterize the complex lacustrine and fluvial dynamics and predict the system's behavior to support informed conservation and planning efforts. We employed a rigorous two-dimensional (2D) hydrodynamic modeling approach using the International River Interface Cooperative (IRIC) software. The model integrated comprehensive topographical, hydrological, and meteorological data to simulate flow behavior over a transient event. The analysis revealed critical insights into the system's vulnerability. Simulation outputs accurately defined areas susceptible to localized flooding and quantified seasonal water level variations. Hydrodynamic analysis confirmed complex flow interactions, including the concentration of maximum velocity and depth within the channel's thalweg and the presence of a downstream backwater effect indicated by an inverse water surface elevation gradient. Furthermore, cross-sectional profiles validated the model's ability to capture asymmetrical channel geometry, which is crucial for bank erosion risk assessment. Supporting land-use analysis highlighted significant land degradation and marshland loss, exacerbating the hydrological response. In conclusion, the IRIC model provides robust predictive capability for evaluating the cumulative impacts of environmental change. A primary recommendation is the urgent need to strengthen the local hydrometeorological monitoring network to enhance data quality and model reliability. The findings facilitate the proactive planning of adaptive strategies, including the construction of protective dikes, targeted reforestation, and essential agricultural adjustments, ensuring the long-term resilience of the Lake Alaotra watershed.

Keywords: Lake Alaotra, Hydrodynamic Modeling, IRIC, Flood Risk, Land Use Change.

1. Introduction

Lake Alaotra, the largest lacustrine system in Madagascar, serves as a critical nexus for the regional economy, biodiversity, and potable water provision within the Alaotra-Mangoro region. Despite this pivotal role, the ecosystem is subjected to escalating anthropogenic pressures and the deleterious effects of climate change. In this demanding environmental context, computational hydrodynamic modeling and simulation emerge as indispensable instruments for systematically characterizing, forecasting, and ensuring the sustainable stewardship of its complex flow regime.

The investigation utilized the International River Interface Cooperative (IRIC) software, a specialized platform for two-dimensional (2D) hydrodynamic modeling, to simulate the intrinsic flow behavior of Lake Alaotra and its contributing riverine network (**Carré et *al*., 2015**). IRIC was judiciously selected for this fluvial and lacustrine modeling task due to its design as a comprehensive simulation environment dedicated to river morphology and flow dynamics. The computational outputs generated by IRIC are readily exportable, facilitating subsequent analysis for the mitigation and prevention of hydrological disasters through the visualization of simulated riverine and inundation outcomes (**Dunlop et *al*., 2018**).

The central objective of this fluvial hydraulics study is the predictive delineation of the flow characteristics of natural watercourses, specifically those associated with the Lake Alaotra system. This endeavor is paramount for developing an evidence-based understanding necessary for the effective management of water resources and associated hydraulic infrastructure, including dams, dikes, and conveyance canals. This research is fundamentally motivated by several strategic imperatives (**McGoldrick et *al*., 2016**) :

- Flood Forecasting and Risk Mitigation : Accurately predicting inundation events to minimize socio-economic and ecological impacts.
- Sustainable Catchment Management : Supporting the long-term ecological and operational viability of the entire watershed.

- Safety of River Navigation : Ensuring secure passage and operability along navigable reaches.
- Aquatic Ecosystem Preservation: Protecting the delicate balance and biological integrity of the lacustrine and riverine habitats.

2. Materials and methods

2.1. Geo-hydrological and climatic characterization of the Alaotra lacustrine system

Lake Alaotra stands as the largest freshwater lacustrine body in Madagascar, constituting a pivotal hydrographic feature within the Alaotra-Mangoro Region (formerly Tamatave Province). Geographically, the lake is situated between the districts of Amparafaravola and Ambatondrazaka, precisely defined by the coordinates 17°28' South latitude and 48°30' East longitude.

The Alaotra system occupies a significant eight percent of Madagascar's total surface area, encompassing an extensive 63,000 hectares (ha). Crucially, this area includes approximately 43,000 ha of expansive marshland, underscoring the system's characteristic wetland-dominated environment and its complex hydrological and ecological mosaic.

Climatically, the region experiences a sub-tropical regime, characterized by a mean annual temperature ranging narrowly from 25°C to 28°C. The average annual precipitation for the catchment is recorded at 1154 mm, influencing the lake's hydroperiod and water balance (**Rabotovao et *al*., 2025**).

2.2. Analysis of land use change (2018–2022) in the Ambatondrazaka and Amparafaravola districts

The analysis of Land Use (LU) maps for the Ambatondrazaka and Amparafaravola districts reveals significant spatio-temporal dynamics across the observed five-year period, indicative of evolving anthropogenic and environmental pressures on the Lake Alaotra watershed.

The classification accuracy of the Land Use maps was assessed using the Kappa coefficient (kappa) and a Confusion index, as summarized in Table 1.

Table 1. Kappa Coefficient and Confusion Index for Land Use Classification Model Accuracy (2018–2022)

Year	**Kappa (κ)**	**Confusion Index**
2018	0.93	0.94
2019	0.91	0.92
2020	0.86	0.91
2021	0.92	0.93
2022	0.93	0.94

The Kappa coefficient (κ), a robust measure of adjusted accuracy that accounts for chance agreement, consistently remained above 0.85 across all years, signifying very high model reliability. Similarly, the Confusion indices, consistently above 0.91, attest to the high overall precision of the classification methodology.

A notable anomaly occurred in 2020, where the kappa (κ) value dropped to 0.86—the lowest in the series. Although still indicating substantial agreement, this decrease suggests a reduced consistency between the classification predictions and ground truth data compared to other years. This perturbation may be attributable to specific data acquisitions issues, changes in the classification algorithm, or real-world disturbances such as an intensified cyclone season, even as the overall precision (Confusion Index : 0.91) remained high. The subsequent recovery in 2021 and 2022 (returning to $\kappa \geq 0.92$) suggests a stabilization or improvement in the methodology. (**Rabotovao et *al*, 2025**)

Table 2 details the quantified changes in the surface area (km^2) occupied by key land use classes within the study area from 2018 to 2022.

Table 2: Comparison of land use area (km^2) within the Ambatondrazaka and Amparafaravola districts (2018–2022)

Year	**2018 (km^2)**	**2019 (km^2)**	**2020 (km^2)**	**2021 (km^2)**	**2022 (km^2)**
Water	213.37	244.00	155.41	256.14	199.34
Forest	1,875.51	2,168.60	3,106.70	1,448.15	1,956.15
Marsh	940.65	404.40	636.20	479.24	595.34
Rice Fields	1,570.07	2,432.50	1,774.30	1,919.39	2,145.39

Year	**2018 (km²)**	**2019 (km²)**	**2020 (km²)**	**2021 (km²)**	**2022 (km²)**
Other Vegetation	467.44	1,251.10	532.25	694.53	587.63
Bare Soil	2,088.49	3,661.70	3,943.92	4,364.82	4,364.82

Observed trends

- Water bodies : Exhibited significant inter-annual fluctuations, peaking in 2021 (256.14 km²) and reaching a nadir in 2020 (155.41 km²). This volatility is likely driven by pronounced seasonal or climatic variations, such as cyclical droughts or high-precipitation events, directly impacting the lacustrine and riverine water surface areas.
- Forest cover : Showed extreme variability, marked by a sharp increase in 2020 (3,106.70 km²) followed by a dramatic decrease in 2021 (1,448.15 km²). Such rapid changes may indicate classification issues, but more importantly, they may reflect intense deforestation and/or reforestation trends within the watershed.
- Marshland : Demonstrated a drastic overall reduction from 940.65 km² in 2018 to 479.24 km²in 2021, suggesting significant wetland degradation or conversion, followed by a minor partial recovery in 2022.
- Rice fields : Displayed a consistent upward trajectory, rising from 1,570.07 km² in 2018 to 2,145.39 km² in 2022, underscoring the ongoing process of agricultural intensification and expansion within the basin.
- Bare soil : Experienced a continuous and substantial increase from 2,088.49 km² in 2018, stabilizing at 4,364.82 km² by 2021–2022. The persistently high and expanding bare soil area is a critical indicator of long-term vegetation loss, likely resulting from severe deforestation, land degradation**,** erosion, and potentially expanding built-up or mining areas.

These Land Use dynamics—particularly the expansion of Bare Soil and Rice Fields alongside the contraction of Marshland—have critical implications for the river hydraulics of the system. Changes in land cover fundamentally alter runoff characteristics, sediment load, and flood propagation patterns, necessitating a thorough understanding of the distinction between fluvial flow (characterized by calmer water surfaces) and torrent regimes (more turbulente and rapid flow), as emphasized in hydraulic studies (**Moriasi et *al*., 2015**).

2.3. Numerical simulation setup

To effectively model the complex hydrodynamics of the Lake Alaotra system, the numerical simulation must be carefully parameterized. This crucial phase begins with the foundational step of grid creation, which defines the spatial domain and resolution for the subsequent flow computations.

2.3.1. Grid creation and domain definition

The numerical simulation necessitates the establishment of a computational grid to discretize the physical domain of the river system.

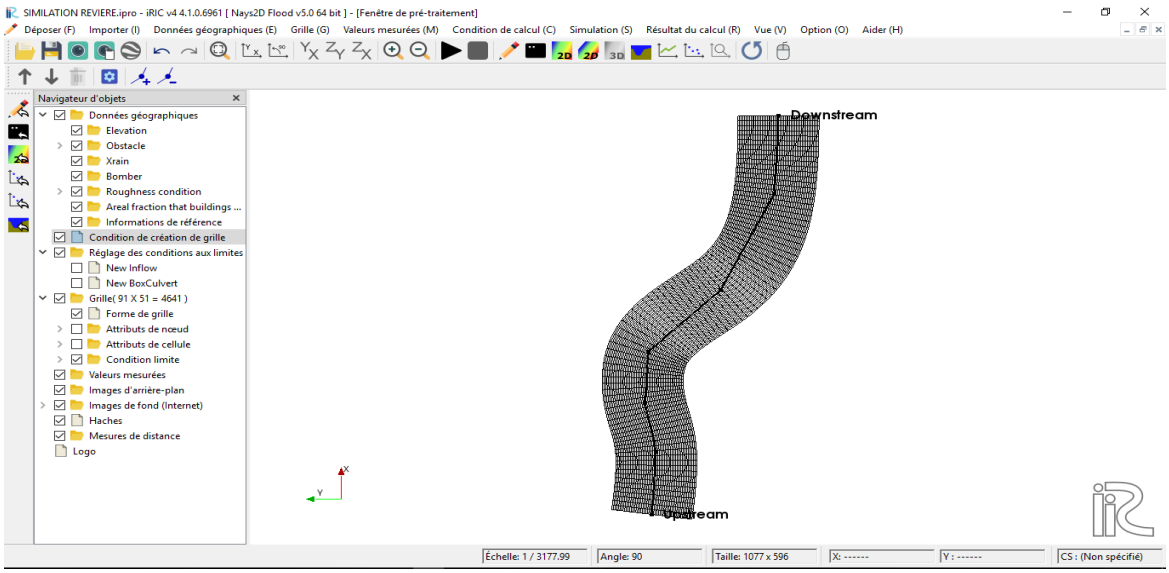

***Figure 1** : Grid creation for the simulation of Lake Alaotra Mangoro on IRIC*

2.3.1.1. Mesh structure and dimensions

The mesh employed is structured, strategically designed to conform to the curvilinear morphology of the meandering river channel, thereby enhancing the accuracy of flow representation near boundaries (**Teng et *al*., 2017**). This grid consists of 91 columns (X-direction) and 51 rows (Y-direction), yielding a total of 4,641 computational cells (91 x 51 = 4641). This discretization forms the fundamental basis upon which all subsequent numerical flow computations—including water velocity and water depth—are executed.

2.3.1.2. Flow orientation

The flow direction within the computational domain is explicitly defined: the Upstream boundary (water entry point) is situated at the bottom of the grid representation, while the Downstream boundary (water exit point) is located at the top. This orientation dictates that the simulated water movement proceeds from the lower section to the upper section, tracking the path of the meandering channel.

2.3.1.3. Interface and model preparation

The model preparation sequence is typically managed through an object browser or similar interface structure, often visible on the left side of the modeling environment. This component provides the systematic steps required for model configuration and validation (**Roget et *al*., 2018**).

2.3.2. Boundary conditions : Transient hydrograph definition

The computational domain requires precise boundary conditions to initiate and drive the simulation. The upstream condition is defined by a transient hydrograph, specifying the time-dependent volumetric flow rate (Q) that governs the system's dynamic response to hydrological events (**Rabotovao et *al*., 2025**).

Table 3 details the discrete time and discharge pairs used to define this critical input.

Table 3: Time and discharge considered in the boundary condition for numerical simulation

Time	0	600	1200	1800	2400	3000	3600	4200	4800	5200	5800	6200	6800	7200	7600
Flow	5000	500	0	460	231	323	369	415	600	2700	3000	1500	400	200	100

Simulation start (t = 0s): high discharge of 5000 m³/s, likely representing an initial strong event (flood or surge).

2.3.2.1. Hydrograph interpretation

The data presented in Table 3 models a complex, multi-peaked hydrological event, such as a severe flood or a controlled water release sequence, utilized to drive the simulation of flow (discharge, velocity, and water depth) over time within the river channel.

- Initial event and rapid recession: The simulation commences at t = 0 s with an extremely high discharge of 5,000 m³/s, likely representing an initial surge or flood peak. This is followed by a sharp and rapid recession, dropping to 500\ m³/s at t = 600s, and momentarily reaching zero discharge at t = 1,200s. The zero flow state potentially indicates a temporary flow cutoff or the model's transient response to an abrupt regulation or event end.
- Secondary peak dynamics : The discharge subsequently begins a gradual rise with minor fluctuations, culminating in a secondary, but substantial, peak of 3,000 m³/s at t = 5,800s. This second maximum suggests a major, delayed inflow event or a subsequent release.
- Final recession : Following the second peak, the discharge enters a protracted recession phase, progressively decreasing to a base flow condition of 100\ m³/s by the end of the simulation period at t = 7,600s.

These prescribed time-series discharge data are essential for providing the dynamic input required by the hydrodynamic model to accurately capture the propagation and attenuation of these transient flow conditions through the simulated river domain.

2.3.3. Roughness condition and simulation time

2.3.3.1. Hydraulic Roughness Parameter

The simulation of flow dynamics requires the definition of a hydraulic roughness coefficient, which accounts for the energy losses due to friction along the channel boundaries. This resistance is critical for accurately modeling flow velocity and water surface elevation.

In this study, the Manning's roughness coefficient (ns) was assigned a value within the narrow range of 0.29 to 0.30. This relatively high coefficient is characteristic of channels with dense vegetation, significant bed irregularities, or heavy sedimentation/debris accumulation, which is plausible given the marshy and dynamic nature of the Lake Alaotra riverine system.

2.3.3.2. Temporal Domain

The total simulation time (or duration) for the transient hydrodynamic event was set to 7,600 seconds. This duration is sufficient to capture the propagation of the defined multi-peaked hydrograph and allow the system's hydraulic response to evolve and stabilize, ensuring a comprehensive analysis of the flood event.

2.3.4. Numerical calculation condition

With the grid and boundary conditions established, the final stage involves defining the calculation parameters. These settings—including temporal discretization, initial conditions, and numerical output controls—are essential for ensuring the stability and practical efficiency of the two-dimensional hydrodynamic solution (**Rabotovao et *al*., 2025**).

The successful execution and stability of the 2D hydrodynamic simulation depend critically on the precise setting of the calculation parameters. These settings, detailed in Table 4, govern the temporal discretization, initial state, and boundary interactions of the numerical model.

Table 4 : Calculation parameters settings

Parameter	Value
Output Time Interval	600 seconds
Calculation Time Step (Δt)	0.02 second
Calculation Start Time	0 second
Initial Water Depth	0 meter
Upstream Boundary Condition (J=1)	Input (Inflow)
Downstream Boundary Condition (J=nj)	Output (Outflow)
Downstream Water Surface Condition	Free Outflow

Analysis of calculation settings

- Calculation time step (Δt) : Set at a highly resolved value of 0.02 seconds. This fine temporal discretization is essential for ensuring numerical stability and achieving high precision, particularly when solving the complex non-linear shallow water equations (Saint-Venant equations) that govern hydrodynamic flow.
- Output Time Interval : Results are recorded and saved at intervals of 600 seconds (10 minutes). This approach manages the substantial data volume inherent in numerical modeling by storing results at practical intervals, sufficient for post-processing analysis while avoiding excessive computational overhead.
- Calculation start time and initial conditions : The calculation commences at t = 0 s with an initial water depth of 0 m. This setting defines a 'dry bed' initial condition, which is a standard procedure for modeling flash flood events, surface runoff, or dam-break simulations where the channel is initially empty or below a measurable depth.
- Domain boundaries (J = 1 and J = n_j): The notation J = 1 (the upstream side of the domain) is designated as the Input (Inflow) boundary, aligning with the prescribed transient hydrograph. Conversely, J = n_j (the downstream side of the domain) is defined as the Output (Outflow) boundary, ensuring that flow leaves the domain appropriately.
- Downstream water surface condition : The implementation of a Free Outflow condition ensures that the water is allowed to exit the domain without the imposition of a fixed water level or artificial head. This prevents the generation of non-physical backwater effects that could inaccurately influence flow dynamics within the computational domain (**Uusitalo et *al*., 2015**).

These parameters collectively define a stable and precise numerical scheme designed to simulate a dynamic flood event over a previously dry channel, reflecting a robust approach for river hydrodynamic modeling.

2.3.5. IRIC numerical calculation settings

This section details the specific numerical methods and controls implemented within the IRIC software to ensure the accuracy, stability, and efficiency of the hydrodynamic simulation (**Yi Hong et *al*., 2021**). These parameters are crucial for fine-tuning the model's behavior and performance.

2.3.5.1. Numerical scheme and stability controls

The Near-site scheme was selected for discretizing the advection terms. This scheme, a type of upwind numerical method, is generally favored in hydrodynamic modeling for its simplicity and ability to maintain numerical stability by reducing spurious oscillations, particularly in regions with steep gradients (**Van Hyfte et *al*., 2023**).

To ensure computational efficiency while maintaining the desired solution accuracy, two parameters govern the iterative convergence process for the water surface solution : The maximum number of internal iterations allowed per time step for converging the water surface solution was set to 10. This limit balances computational speed against the required level of accuracy.

A relaxation coefficient of 0.8 was employed. This factor is used in iterative solvers to adjust the calculated water surface elevation between iterations, aiding in the convergence process and enhancing the model's stability.

The model enforces a minimum permissible water depth of 0.01 meter. This threshold is essential for avoiding computational singularities (division by zero) that can occur in the momentum equations when calculating flow velocity in dry or near-dry cells.

2.3.5.2. Viscosity, parallelization, and domain options

The viscosity coefficients were set as follows: Coefficient A = 1 and Coefficient B = 0. These parameters govern the representation of turbulent effects or effective viscosity in the model. This specific setting configuration corresponds to the model's chosen turbulence closure formulation.

The simulation was configured to use 1 thread for parallel computation. While using a single thread simplifies execution and output, utilizing multiple threads is typically recommended for large domains to significantly reduce processing time.

The option for Building Flooding was Disabled. This indicates that the simulation focused purely on the inundation dynamics within the primary defined channels and adjacent terrain, without incorporating the detailed hydraulic resistance effects of structures or buildings on the flood wave propagation.

2.3.6. Roughness condition and grid creation setting

To finalize the model setup, the physical parameters that define flow resistance must be integrated with the spatial discretization. This section details how the Manning's roughness coefficient (n) was mapped onto the computational grid to accurately represent the riverbed's frictional effects within the simulation domain.

2.3.6.1. Domain definition and obstacle representation

The spatial setup for the hydrodynamic simulation is visualized in Figure 2 , which details the configuration of the computational grid and the initial assignment of the roughness condition.

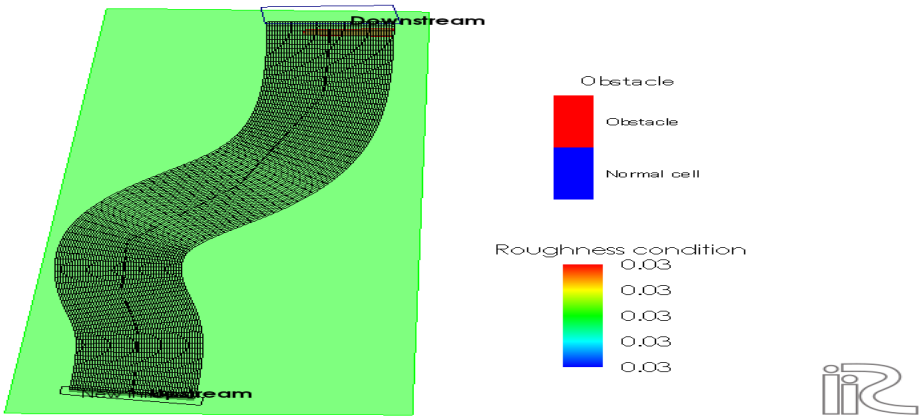

Figure 2: Obstacles and roughness condition value

The generated grid is composed of cells categorized by flow status. The legend designates two types of cells: Red cells are designated as Obstacle cells (representing zones that locally impede or block flow, such as artificial banks or levees), while Blue cells correspond to Normal cells (representing the active flow zone).

Crucially, in the depicted computational domain, no red obstacle cells are present. This implies that the initial analysis or base simulation models the river segment as an unobstructed, naturally evolving channel, without incorporating the influence of specific hydraulic structures within the grid boundaries.

2.3.6.2. Uniform hydraulic roughness

The riverbed resistance, parameterized by the Manning's roughness coefficient (n), is applied uniformly across the entire computational domain, represented by a single value of 0.03. This coefficient is characteristic of a natural riverbed composed of fine gravel or stabilized by short grass (**Mandal & Choudhury, 2016**). The uniform color scale across the domain visually confirms this consistent roughness assignment.

2.3.6.3. Simulation utility

The resulting model—defined by a well-structured mesh following a meandering path, the absence of fixed obstacles, and a uniform roughness coefficient—is particularly well-suited for several analytical applications :

- Comparative analyses : Serving as a baseline 'pristine' scenario for comparing hydraulic behavior before and after hypothetical river engineering interventions (e.g., dam construction, levee placement).
- Fundamental dynamics studies : Illustrating and analyzing the fundamental effects of channel sinuosity on river dynamics, including velocity distribution and secondary flow patterns.
- General modeling : Providing a foundation for preliminary simulations of flood wave propagation and sediment transport under idealised conditions.

2.4. Data analysis

With the numerical simulation successfully executed using the defined parameters, the next critical phase involves analyzing the model outputs. This process focuses on extracting key hydraulic variables to interpret the river's dynamic response to the imposed hydrograph, starting with the spatial and temporal distribution of flow velocity.

2.4.1. Analysis of simulated velocity field

The analysis of flow velocity (V) is paramount, as this derived parameter directly reflects the energy and momentum distribution within the river system.

The simulation outputs provide spatially and temporally explicit velocity fields , which are essential for several key hydraulic assessments:

- Erosion and deposition : High-velocity zones (typically found on the outer bends of meanders) correlate with potential bank erosion and scour, while low-velocity zones (inner bends, floodplains) indicate areas prone to sediment deposition.
- Safety and navigation : Velocity magnitude is a critical factor for assessing the safety of river navigation and determining the forces exerted on hydraulic structures.
- Mixing and transport : Velocity distributions govern the mixing and dispersion of pollutants, nutrients, and heat throughout the water column, impacting water quality and aquatic habitat viability.

The calculated velocity maps are therefore used to understand the complex secondary circulation patterns characteristic of meandering channels, where flow is highest near the outer bank at the surface and near the inner bank at the bed, a phenomenon crucial for morphological understanding.

The simulated velocity is presented by magnitude, ranging from very low velocities (~ 0.01m/s, blue zones) to high velocities (up to 9.21m/s, red zones), as shown in Figure 3.

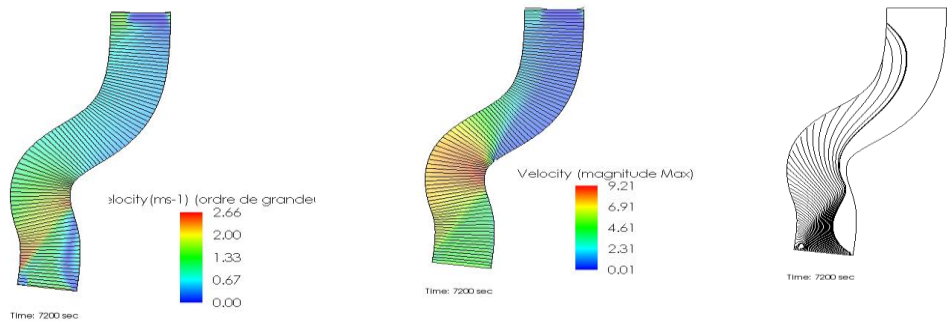

Figure 3 : *Simulated velocities in the analysis domain*

2.4.1.1. Velocity magnitude and spatial variability

The spatial distribution of velocity clearly demonstrates the characteristic hydraulic behavior of a sinuous (meandering) channel (**An et *al*., 2015 ; Dimitriadis et *al*., 2018**) :

- High-velocity zones (red/orange) : The maximum velocity zones (up to 9.21 m/s) are consistently located along the outer (concave) curve of the meanders (e.g., downstream of the lower and upper bends). This phenomenon is physically explained by the centrifugal force that pushes the faster-moving water mass outward, concentrating flow and increasing speed at the outer bank (**Bader et *al*., 2016 ; Le Moal et *al*., 2019**). These regions are typically prone to intense bank erosion and scour.
- Low-velocity zones (light blue/green): Conversely, zones of significantly lower velocity are observed on the inner (convex) bends or proximal to the riverbanks. These regions experience reduced shear stress and are highly susceptible to sediment deposition (**Cooper et *al*., 2018**).

2.4.1.2. Flow direction and momentum

The velocity vector arrows super-imposed on the contour map indicate both the direction and intensity of the flow (**Codling et *al*., 2018**). The arrows follow the sinuous channel shape, confirming that the current successfully adapts to the meandering path.

- The longer and redder the arrows, the higher the flow velocity, reinforcing the pattern of flow concentration on the outer bends.
- The streamline distribution appears denser at the channel entrance, suggesting the impact of the initial high discharge condition, and exhibits expected curvature and outward concentration throughout the bends, illustrating the centrifugal effect on the flow dynamics.

2.4.1.3. Hydraulic Implications

This realistic simulation of spatial velocity variability within a sinuous channel is critical for several engineering and environmental applications :

- Morphological evolution : The model can be used to accurately locate potential erosion zones (concave banks) and deposition zones (convex banks), informing predictions of long-term riverbed and bank stability.
- Flood and infrastructure management : Understanding high-velocity regions is essential for flood risk management and for the appropriate sizing and placement of hydraulic infrastructure to withstand expected hydrodynamic forces.
- Ecological assessment : Velocity heterogeneity is a key factor influencing habitat suitability, sediment transport capacity, and the dispersion of contaminants.

The overall flow distribution indicates good model stability, typical of well-executed simulations of natural river regimes (**An et *al*., 2015**).

2.4.2. Analysis of elevation and depth

Following the velocity analysis, interpreting the simulated water surface elevation (Z) and flow depth (h) is essential. These parameters directly quantify the extent of inundation and the magnitude of the flood wave propagating through the channel. Analyzing depth is crucial for assessing potential flood risk and its impact on surrounding infrastructure and land use (**Rabotovao et *al*., 2025**).

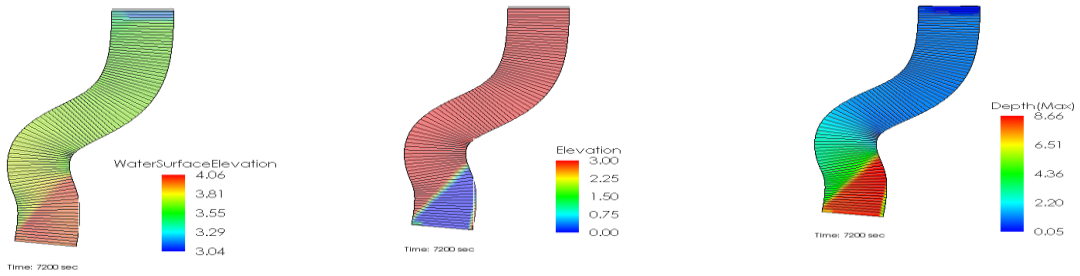

Figure 4 : Simulated elevation and depth values in the lacustrine system

The visualization in Figure 4 provides a comprehensive view of the static and dynamic vertical dimensions of the simulated water body:

- Elevation (ground): This base layer represents the bathymetry and topography of the riverbed and the surrounding floodplain. The absolute ground elevation is the foundational input used to determine the flow direction and potential inundation areas when compared to the water surface.

- Water surface elevation (Z): This parameter represents the absolute height of the water surface relative to a fixed datum (e.g., mean sea level). The simulation accurately models the downward slope of the water surface, reflecting the gravitational gradient that drives the flow from the upstream boundary to the downstream boundary.
- Flow depth (h): Calculated as the difference between the Water Surface Elevation and the Ground Elevation (h = Z - Ground Elevation), the flow depth directly quantifies the local water column thickness. The maximum depth observed is critical for determining the severity of flooding and the potential impacts on submersed infrastructure.

The spatial analysis of these values is crucial for:

- Flood mapping: Identifying all areas where the Water Surface Elevation exceeds the Ground Elevation of the adjacent terrain, thereby defining the extent of inundation.
- Infrastructure safety: Determining the water depth and pressure head relative to dams, dikes, and irrigation canals.
- Sediment transport: Depth is a key input in the governing equations for sediment transport capacity, as deeper flows often carry larger sediment loads.

The simulation's ability to accurately capture the spatial variability of Z and h across the irregular terrain of the lacustrine and riverine system validates its utility for flood risk management and water resource planning (**Rabotovao et *al*., 2025**).

2.4.2.1. Water surface elevation analysis

The simulated Water Surface Elevation (Z) provides crucial insights into the hydraulic head driving the flow and the longitudinal profile of the flow event.

Elevation magnitude and gradient

The color scale visualization indicates the range of computed water surface elevations across the domain (**Munawar et *al*., 2022**) :

- Maximum surface elevation (red): Approximates 4.06 meters.
- Minimum surface elevation (dark blue) : Approximates 3.04 meters.
- Elevation gradient : The shift from red to dark blue represents the overall change in hydraulic head across the simulated reach.

Flow dynamics and hydraulic behavior

The flow direction is inferred from the elevation gradient. In this representation, the flow proceeds from top to bottom (north to south) :

- Upstream Inlet: Located at the top of the domain, characterized by lower elevations (blue/green zones, closer to 3.04 m).
- Downstream Outlet: Located at the bottom of the domain, characterized by higher elevations (yellow/red zones, approaching 4.06 m).

The observation that the water level rises downstream (from blue to red) is contrary to the typical gravitational flow in a river, where the elevation usually drops in the downstream direction. This suggests the presence of a controlling hydraulic feature or condition, such as:

- Fixed downstream water level : The downstream boundary condition might be a fixed elevation (e.g., 4.06 m), causing a backwater effect that raises the upstream water level.
- Local obstruction or high resistance : A significant hydraulic resistance (e.g., a submerged obstacle, a pronounced hydraulic jump, or a sudden and substantial increase in channel roughness/narrowing not explicitly mapped) near the outlet could cause water to pile up.

The visualization, potentially through black lines (representing either isolines of elevation or streamlines), further helps to map the variation and direction of the surface elevation relative to the sinuous meandering riverbed (**Munawar et *al*., 2022**).

2.4.2.2. Bed elevation analysis

The Bed Elevation (or Bottom Altitude) component of the simulation data reveals the topographical structure (bathymetry) of the channel and its surrounding floodplain, which fundamentally controls the flow pathway and capacity.

Altitude Magnitude and Gradient

The color scale on the right of the figure shows the variation in the ground and submerged bed elevation:

- High zones (red): Approximating 3 meters.
- Low zones (blue): Approximating 0 meters.

The overall gradient suggests that the bed is lower downstream (towards the bottom of the image). This is the typical configuration for natural gravitational flow, where the energy gradient causes the flow to proceed from the higher upstream elevation to the lower downstream elevation (**Neal et *al*., 2019**).

Channel topography and morphodynamics

The sinuous shape of the channel is characteristic of a fluvial meander, where localized altitude variations are the result of ongoing erosion and sedimentation processes :

- Erosion (scoured areas) : Indicated by blue shades (deeper bed elevation), these areas represent locations where the stream power has been sufficient to scour and remove bed material.
- Deposition (raised areas) : Indicated by red shades (higher bed elevation), these areas represent sediment accumulation due to reduced local flow velocity.

The black lines or streamlines confirm the downstream flow direction (converging towards the bottom of the image).

Hydrodynamic interpretation in meander bends

The classic principles of river geomorphology dictate the flow-bed interactions within a curve:

Feature	Location	Associated Process	Elevation
Scour Zone	Concave side (Outer curve)	Erosion is strongest	Lower (Blue)
Bar Formation	Convex side (Inner curve)	Deposition is strongest	Higher (Red)

This simulated topography is essential for understanding the morphological evolution of the riverbed and assessing the long-term stability of the channel.

Implications for water level

The previous section (2.4.2.1) noted an unexpected rise in water surface elevation downstream (red zone in the water surface map). While the bed elevation shows a typical drop downstream, the significant disparity between the high water surface elevation (up to 4.06 m) and the low bed elevation (down to 0 m) in the downstream area suggests a large water depth accumulation. This accumulation (or hydraulic head buildup) may indeed indicate a risk of localized flooding or hydraulic accumulation caused by factors external to the immediate bed gradient, such as :

- A constriction just downstream of the simulated domain.
- A backwater effect due to a fixed high water level at the system's outlet.
- A significant flow slowdown caused by high friction or resistance.

2.4.2.3. Analysis of flow depth

The Flow Depth (h) output is a critical variable derived from the difference between the computed Water Surface Elevation and the Bed Elevation. Its spatial distribution reveals areas subject to the highest hydraulic pressure and potential inundation risk.

Depth magnitude and spatial distribution

The color scale visualization indicates the range of computed flow depths across the domain (**Sharma & Lamichhane, 2020**) :

- Maximum depth (red): Approximates 8.66 meters.
- Minimum depth (dark blue): Approximates 0.05 meters.

The scale confirms that warmer colors (red, orange) correspond to greater flow depths, while cooler colors (blue) indicate shallower zones.

Hydro-morphological correlation

The spatial distribution of flow depth directly correlates with the expected hydro-morphological behavior of a meandering channel :

- Shallow zones (blue) : These zones, often found on the inner (convex) side of channel curves, are symptomatic of sediment deposition where flow velocity is lowest. The presence of shallow areas near the outer banks in some regions (blues often on the outer side of the curves) suggests complex secondary flow patterns or localized effects not conforming strictly to the classic meander model, possibly due to upstream influences or heterogeneous bed material.
- Deep zones (red) : The occurrence of maximum depth (up to 8.66\ m) in the downstream left section is significant. This localized deep zone likely corresponds to a water accumulation area, potentially caused by a substantial channel widening, a marked slowdown of flow velocity, or a pronounced backwater effect as the flow exits the domain (**Sharma & Lamichhane, 2020**).

Flow dynamics and meander evolution

The simulated deep zones, often concentrated within specific channel parts, emphasize the role of channel curvature and bed topography in concentrating flow energy. The overall sinuous profile confirms the natural migration tendency of the watercourse, which inherently promotes lateral erosion on the concave banks, deepening the channel, and deposition on the convex banks, shallowing the flow.

Where flow vectors are present (even if thin), they confirm that the current follows the channel's curvature, demonstrating the physical realism of the simulation. This depth analysis is vital for predicting scour, determining flood capacity, and assessing the stability of channel banks.

2.4.3. Upstream velocity situation

Understanding the velocity field at the upstream boundary is crucial as it governs the momentum input to the entire simulation domain. This section specifically analyzes the calculated velocity magnitudes and vector directions near the inlet to ensure the model accurately reflects the inflow condition set by the transient hydrograph (**Rabotovao et *al.*, 2025**).

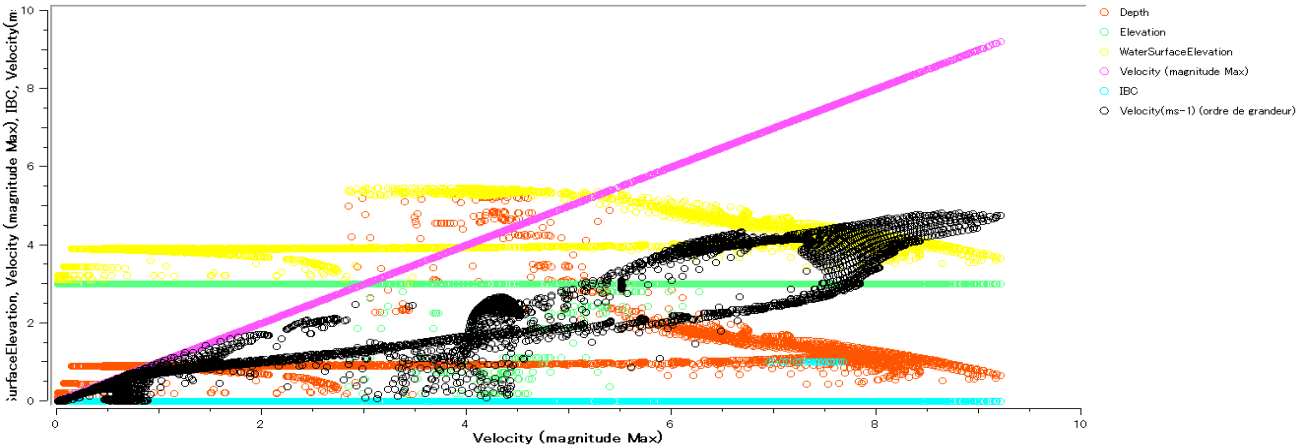

Figure 5 : *Nonlinear relationship between velocity and depth, actual velocity, and overlay*

The upstream boundary condition significantly influences the propagation of the flow wave throughout the domain. Figure 5 presents a critical cross-variable analysis of the simulated outputs, illustrating the complex relationship between flow velocity and flow depth, likely captured near the inlet or along the initial reach.

2.4.3.1. Nonlinear hydrodynamic relationship

The observed scatter plot reveals a nonlinear relationship between velocity (V) and depth (h). Instead of a simple proportional increase, the data suggests that as velocity increases (indicating acceleration), the depth tends to stabilize or even slightly decrease. This behavior is characteristic of hydraulic controls such as :

- Steep gradients (supercritical flow) : In highly sloped areas, flow accelerates, and depth decreases (**Rajeshkumar et *al.*, 2018**).
- Channel contraction (constriction) : As the flow area is reduced, velocity must increase to maintain continuity, often with an associated reduction in depth.
- Energy conversion : The system is converting potential energy (depth) into kinetic energy (velocity) due to acceleration.

2.4.3.2. Data clustering and model validation

The visualization of the cluster of black dots (actual velocity data) highlights specific groupings, indicating discrete zones or flow regimes within the simulated system that exhibit characteristic hydraulic behaviors.

The utility of this multi-variable overlay is paramount for model validation and assessment (**Tammeorg et *al.*, 2017**) :

- Qualitative Evaluation : It enables a qualitative assessment of the model's response based on the defined Initial and Boundary Conditions (IBCs), local topography, and the resulting depth profile.
- Consistency Check : The graph allows researchers to verify the consistency of simulated data and ensures that the model adheres to expected physical laws (e.g., Froude number dynamics) under varying conditions.
- Critical Zone Identification : Deviations from the reference (linear) line (represented by the purple diagonal) highlight nonlinear or segmented behaviors, which can identify hydraulically critical zones characterized by exceptionally high velocities or low depths that require specific management attention.

In summary, this graphical analysis underscores the complex, non-uniform interaction between velocity, water surface, topography, and depth in the modeled river system, making it an indispensable tool for adjusting and validating the final hydraulic model.

2.4.4. Analysis of downstream velocity situation

Analyzing the velocity field at the downstream boundary is crucial for understanding how the flow exits the computational domain. This section specifically examines the calculated velocity magnitudes and vector directions near the outlet to verify consistency with the imposed downstream boundary condition (free outflow) (**Rabotovao et *al*., 2025**).

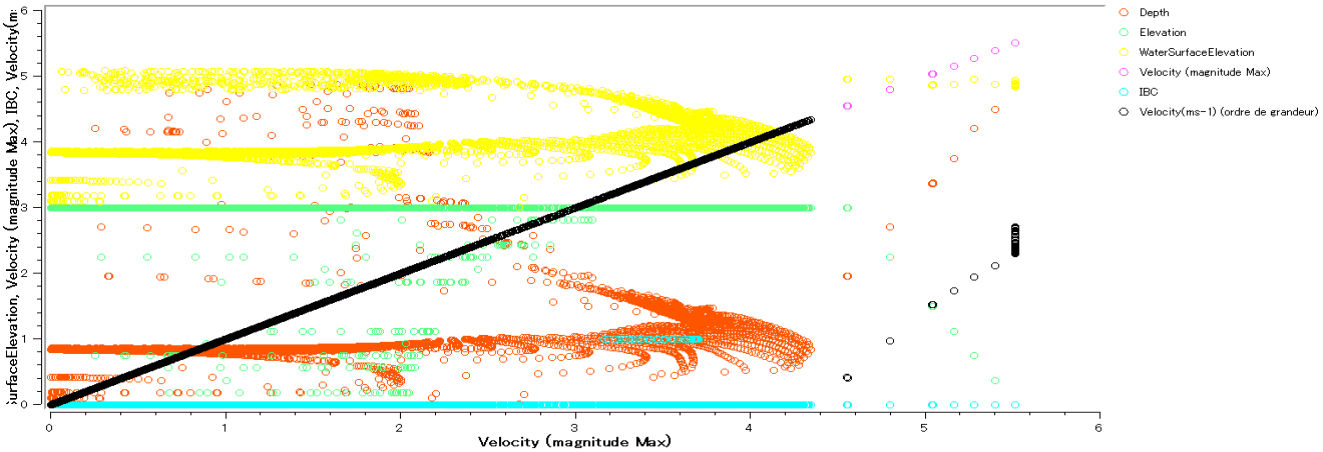

Figure 6 : *Downstream velocity situation and hydraulic variable relationship*

The analysis of the velocity field at the downstream boundary is essential for verifying the consistency of the model's output as the flow exits the computational domain. Figure 6 presents a multi-variable scatter plot illustrating the relationship between hydraulic variables near the outlet.

2.4.4.1. Correlation between hydraulic variables

The scatterplot displays a robust consistency between the simulated hydraulic variables near the downstream boundary (**Zeiger et *al*., 2021**):

- Depth vs. velocity : The data points reveal a trend where depth appears to decrease as velocity increases. This inverse relationship is physically plausible and consistent with the principle of energy conservation in open channel flow, where flow is forced to accelerate (high velocity) in areas of reduced cross-sectional area or shallow depth.
- Elevation (bed) : The bed elevation data appears organized into distinct horizontal levels, potentially representing specific topographic steps or terraces within the simulated river corridor, reflecting the complexity of the channel's bathymetry.
- Water surface elevation : The free surface data exhibits a behavior parallel to the bed elevation data but is consistently higher, accurately representing the flow depth above the channel bed. Shallow depths are implied where the free surface points are closest to the bed elevation points.

2.4.4.2. Model performance and boundary condition check

The purple points (maximum velocity) are correctly situated in the upper-right portion of the graph, confirming that the highest computed velocities align with the expected high-energy conditions, thus validating the physical realism of the calculation.

The cyan points (representing Boundary Conditions, IBC) form very regular lines along the Y-axis. This precise horizontal alignment strongly suggests that the model is correctly reading and utilizing imposed constant values (e.g., a fixed reference stage or elevation) at the boundary, confirming the stability and proper application of the downstream boundary condition (likely a fixed elevation or a known relationship to a reference point).

The black points, representing order-of-magnitude velocities (potentially at key monitoring points), show a well-aligned, upward-sloping linear trend. This linearity suggests a fundamental or technical relationship (potentially a calibration reference or a defined rating curve) that the simulated flow is accurately adhering to.

In conclusion, Figure 6 serves as a critical diagnostic tool, illustrating the model's stability, verifying the execution of the boundary conditions, and confirming the inverse hydraulic relationship between velocity and depth near the lake outlet.

2.4.5. Depth situation : Interrelationship with velocity and elevation

Following the comprehensive analysis of velocity, the final critical step is to analyze the simulated flow depth (h) across the domain. The depth is the primary indicator of the hydraulic loading on the riverbed and floodplains, directly revealing the potential for inundation and the magnitude of the flood wave propagating through the Lake Alaotra system (**Rabotovao et *al*., 2025**).

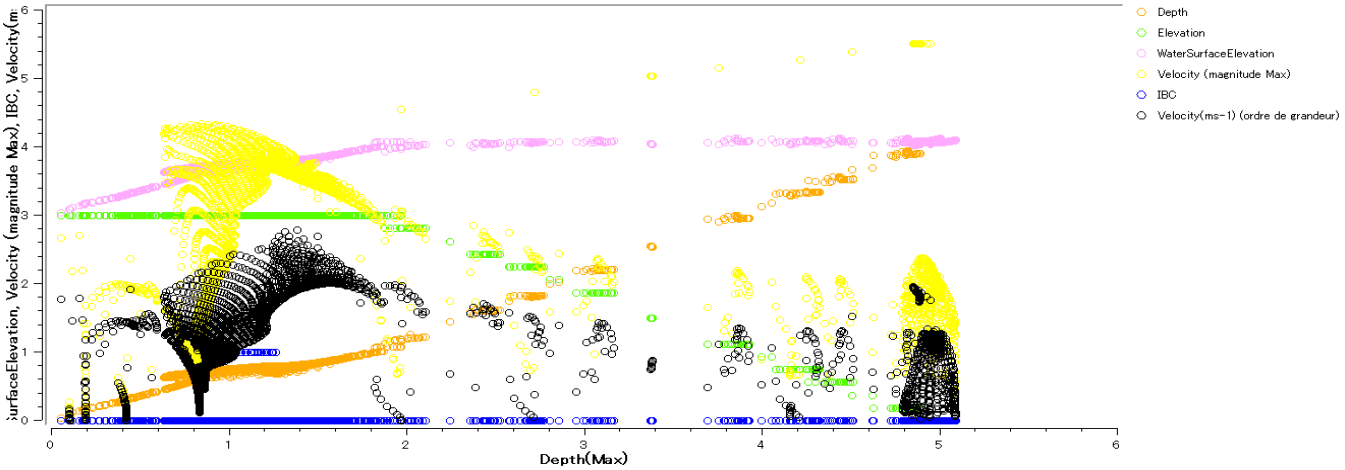

Figure 7 *: Depth and velocity situation*

The final critical diagnostic step involves analyzing the simultaneous interaction between flow Depth (h), Velocity (V), and Elevation (Z). Figure 7, a multi-variable scatter plot, provides essential insights into the system's combined hydrodynamic response.

2.4.5.1. Depth-velocity correlation

The plot illustrates a complex, segmented relationship between depth and velocity, represented by the black and orange points :

- Initial acceleration phase : Velocity tends to increase with depth up to an approximate threshold of 1.5 to 2.0 meters. This initial trend is typical of high-flow zones within the main river channel where the conveyance capacity increases with depth.
- Plateau or decay phase : Beyond this threshold depth, velocity appears to plateau or slightly decrease. This shift suggests the flow may be transitioning from the main channel onto a floodplain, where flow spreading increases wetted perimeter and friction, leading to a stabilization or reduction in average velocity despite increasing depth (**Yuen et *al*., 2021**). This phenomenon may also result from local channel constrictions or slope effects causing changes in flow regime.

The observation that clusters of orange points (maximum velocity) appear at various depths confirms that the highest velocities do not always align with the maximum flow depth, underscoring the dominant influence of local energy gradient and channel geometry (roughness, slope, constrictions) over depth alone.

2.4.5.2. Elevation and boundary condition consistency

The green points (Bed Elevation) display a relatively constant value across certain depth ranges, indicating zones with a flat or gently sloped riverbed. The purple points (Water Surface Elevation) often run parallel to the bed elevation points, signifying regions of uniform or steady flow where the hydraulic gradient remains consistent.

The persistence of blue points (Initial/Boundary Conditions, IBC) at the bottom of the graph is expected. These points represent cells or nodes where initial or fixed values (e.g., zero initial velocity or fixed downstream stage) are imposed, thus forming a stable baseline and validating the correct implementation of the boundary parameters.

2.4.5.3. Model quality and variability

The overall point entanglement and the appearance of clusters or point clouds indicate areas of homogeneous hydraulic behavior (e.g., stable channel sections), whereas scattered data points reflect significant spatial variability within the system (e.g., turbulent zones, flow bifurcations, or rapid transitions). This visualization is essential for :

- Quality assurance : Analyzing the consistency of simulated elevations and velocities.
- Risk identification : Identifying high-flow zones crucial for erosion or flood risk assessment.

- Anomaly detection : Detecting potential issues such as poorly defined boundary conditions or hydraulic instability in dry cells (**Yuen et *al.*, 2021**).

The graph effectively demonstrates the complex, multi-dimensional interactions between the key hydraulic variables, which is fundamental to validating the performance of the 2D hydrodynamic simulation model.

3. Results and discussion

3.1. Hydrodynamic modeling for sustainable water resource management in the lake Alaotra-Mangoro system

The sustainable management of water resources within the critical Lake Alaotra-Mangoro system is an imperative for securing the ecological and socio-economic stability of the eastern region of Madagascar. This study employed a rigorous hydrodynamic modeling and simulation approach to characterize the intricate lake dynamics and predict its behavior in the face of ongoing climatic and anthropogenic pressures.

The investigation utilized the International River Interface Cooperative (IRIC) software, implementing a two-dimensional (2D) numerical model that integrates essential topographical, hydrological, and meteorological input data. The simulation results provide crucial insights into the system's vulnerability and response dynamics, specifically highlighting flood-prone areas, seasonal water level variations, and the potential cumulative impacts of climate change on the entire watershed.

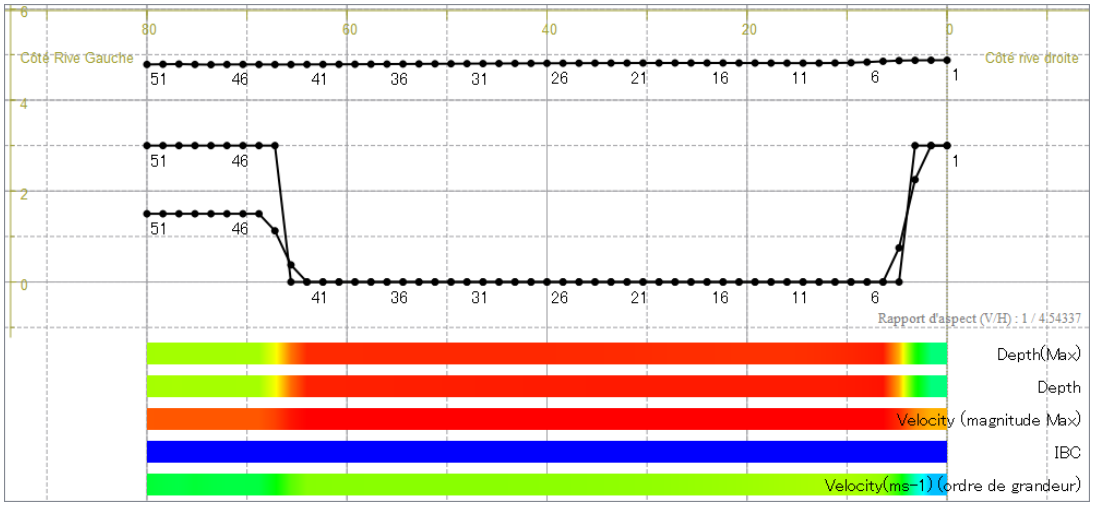

Figure 8 : Physical quantities along the section

The predictive capability of the IRIC model, particularly through the visualization of physical quantities along a characteristic section (Figure 8), proved highly relevant for dissecting the lacustrine dynamics and complex flow interactions. These outputs facilitate the proposition of appropriate, evidence-based management strategies and provide critical support for local decision-makers.

3.1.1. Analysis of cross-sectional flow dynamics

The detailed visualization of the physical quantities along a characteristic river cross-section (Figure 8) serves as a critical validation point for the model's accuracy.

The analysis of the cross-section reveals the governing natural fluvial dynamic :

- Flow concentration : The profiles for maximum depth (Max) and maximum velocity magnitude are both highly concentrated in the central region (the red zone), defining the deep channel (thalweg). This pattern, where the highest speeds align with the deepest part of the bed, confirms the principle of flow seeking the path of least resistance and maximum momentum (**Sylvain Biancamaria et *al.*, 2019**).
- Containment and safety : The banks (left and right) exhibit significantly lower depths and velocities. This is a crucial observation, indicating that under the simulated discharge conditions, the flow is effectively contained within the main channel, providing a natural safety margin against overflow into the adjacent floodplains.

Technical Notes : The visualization employs a vertical-to-horizontal aspect ratio (V/H) of 1 / 454.337, resulting in strong vertical exaggeration. This is a standard graphical technique used to enhance the visibility of subtle variations in the channel bathymetry and water surface profile. The results are characteristic of a successful unsteady simulation relevant for flood management and hydraulic design.

3.1.2. Model limitations and adaptive strategy

While the IRIC model successfully dissected the complex dynamics of the system, the accuracy and predictive reliability of the numerical outputs are fundamentally constrained by the quality and resolution of the input data.

Consequently, a primary recommendation stemming from this study is the urgent requirement to strengthen and expand the local hydrometeorological monitoring network to ensure long-term data consistency and quality (**Rabotovao et *al*., 2025**).

The robust predictive capability of the simulation concerning the adverse effects of climate change is a significant asset, enabling the proactive planning of suitable adaptive developments to enhance system resilience. These strategic interventions include:

- The necessary construction of protective dikes.
- Targeted reforestation efforts within the catchment area to stabilize slopes and reduce runoff.
- Essential agricultural adjustments to mitigate erosion and limit adverse hydraulic impacts (**Rabotovao et *al*., 2025**).

3.2. Analysis of asymmetrical channel topography and hydraulic concentration

The simulation output provides a detailed Topographic Profile across a critical river section, revealing the channel's inherent geometric characteristics and the resultant hydraulic distribution.

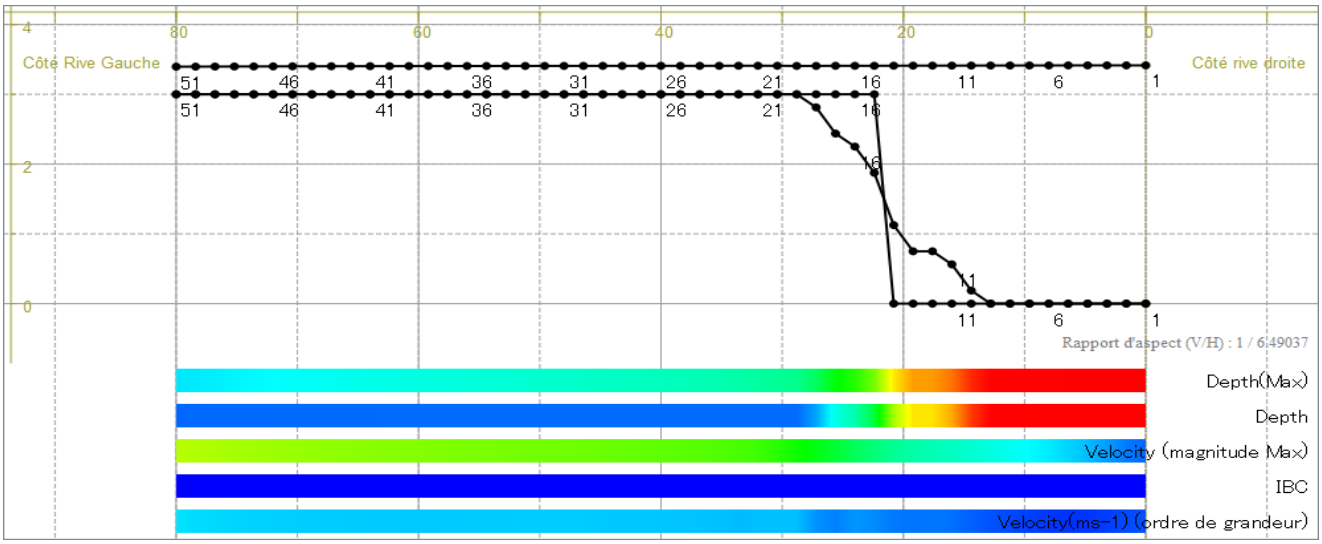

Figure 9 : Topographic profile of the left and right banks

3.2.1. Asymmetrical channel geometry

The cross-sectional geometry exhibits significant asymmetry. Beginning from the Left Bank Side, the bed maintains a relatively flat profile for approximately 20 to 25 meters. This is followed by a steep slope observed between points 21 and 6, which defines a pronounced embankment or transition zone. Finally, the Right Bank Side flattens again. This geometry confirms an asymmetrical bed where the minor bed is deeply incised near the steeper right bank.

3.2.2. Hydraulic distribution and flow concentration

The superimposed hydraulic variables—illustrated by the colored legend—confirm the concentration of momentum and energy in the deepest part of the channel (**Teuling et *al*., 2017**):

- Depth and main flow zone : The simulated maximum depth (depth max, red zone) is concentrated in the center, indicating the main active flow zone. The profile clearly defines a narrow and deep channel (the thalweg) positioned near the right bank.
- Velocity magnitude : High velocities (velocity magnitude max, cyan to red) are strongly concentrated in the same region where the bed is deepest. This concentration of high flow speed in the deepest part of the bed is a fundamental hydraulic principle, demonstrating that the flow seeks the path of least resistance and maximum conveyance.

The model accurately captures the spatial variation in depth and speed across the section, confirming that this profile constitutes an asymmetrical channel with the bed deeply incised near the right bank.

3.2.3. Simulation utility

This specific cross-sectional profile provides data critical for several practical applications :

- Hydraulic model calibration : It is essential for verifying the model's ability to replicate observed flow-bed interactions.
- Bank erosion risk analysis : The concentration of high velocity and deep water near the steep right bank directly identifies this area as being highly susceptible to bank erosion and scour.
- River management and restoration : The geometry and flow distribution data are foundational for designing effective channel stabilization or restoration projects.

3.3. Analysis of watercourse cross-section and bed elevation

The final cross-sectional profile (Figure 10) provides a detailed visualization of the bed elevation and simulated hydraulic variables, offering critical insights into the flow geometry and energy distribution within the channel.

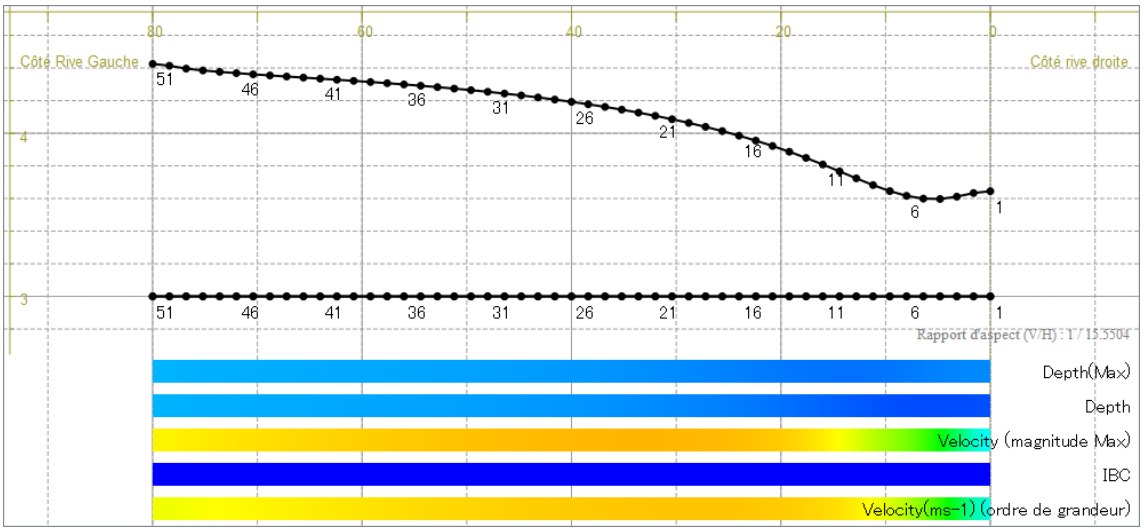

Figure 10 : **Cross-section of the watercourse and bed elevation**

3.3.1. Geometric profile and hydraulic representation

The plot displays the spatial discretization along the horizontal axis (X), numbered from 1 to 51, representing measurement points across the width of the watercourse from the left bank to the right bank. The vertical axis (Y) denotes the elevation of the riverbed (likely in meters).

Two primary curves define the hydraulic state :

- Top Curve: Represents the riverbed profile (bathymetry).
- Bottom Curve: Represents the free surface of the water, corresponding to the simulated water level.

The difference between these two curves at any point provides the flow depth (h).

3.3.2. Bed morphology and flow dynamics

The channel bed depth exhibits a non-uniform profile : the bed is higher near the left bank and gradually lowers toward the right bank. This profile suggests a sloping or asymmetrical channel rather than a deeply incised central thalweg.

The accompanying horizontal colored bars represent critical hydraulic quantities:

- Depth (Max) : The maximum depth recorded.
- Velocity (magnitude Max) : The maximum water velocity observed (in m/s).
- Velocity (order of magnitude) : The general flow velocity distribution, indicated by colors (e.g., green-yellow colors denote fast flow zones).

The analysis reveals that the highest velocities are concentrated in the center-right section of the channel, which corresponds to the area where the flow depth is greatest. This strong correlation between maximum velocity and maximum depth confirms the concentration of flow momentum in the deepest part of the conveyance area. This concentration of energy in the center-right is a sign of potential erosion in that zone due to increased shear stress.

This detailed cross-section is essential for model validation, accurately depicting the complex interplay between the fixed topography and the dynamic simulated flow conditions (**Rabotovao et *al.*, 2025**).

4. Conclusion

This study has demonstrated the importance of 2D hydrodynamic modeling, using IRIC software, in analyzing the behavior of Lake Alaotra and its watershed. By integrating topographic, hydrological, and climatic data, we were able to accurately simulate water flows, identify risk zones (erosion, flooding, sedimentation), and evaluate river dynamics in a sinuous channel.

Our simulations show that the shape of the riverbed, roughness, and discharge variations have a direct impact on water speed and depth, as well as environmental risks. This type of modeling not only allows visualization of climate change effects (flood intensification, seasonal variations), but also enables virtual testing of different management scenarios (dike placement, ecological restoration, reforestation).

However, the model's quality strongly depends on the accuracy of input data. It is therefore recommended strengthening the local hydromelteorological measurement network to improve model calibration and validation.

In conclusion, digital simulation is a powerful decision-support tool for local authorities and environmental managers. It promotes a proactive and sustainable approach to water management, which is essential for preserving the unique ecosystem of Lake Alaotra and for the harmonious development of the Alaotra-Mangoro region.

References

1. An, H., Yu, S., Lee, G., & Kim, Y. (2015). Analysis of an open source quadtree grid shallow water flow solver for flood simulation. *Quaternary International*, *384*, 118–128. https://doi.org/10.1016/j.quaint.2015.01.032
2. Bader, J.-C., Belaud, G., Lamagat, J.-P., Ferret, T., & Vauchel, P. (2016). Modélisation de propagation d'écoulement entre lits mineur et majeur sur les fleuves Sénégal et Niger. *Hydrological Sciences Journal*, *62*(3). https://doi.org/10.1080/02626667.2016.1148815
3. Carré, C., Deroubaix, J.-F., Deutsch, J.-C., & Haghe, J.-P. (2015). *Pratiques et DCE autour de l'Orge*. https://doi.org/10.26047/PIREN.rapp.ann.2009.vol31
4. Codling, G., Sturchio, N. C., Rockne, K. J., Li, A., Peng, H., Tse, T. J., Jones, P. D., & Giesy, J. P. (2018). Spatial and temporal trends in poly- and per-fluorinated compounds in the Laurentian Great Lakes Erie, Ontario and St. Clair. *Environmental Pollution (Barking, Essex: 1987)*, *237*. https://doi.org/10.1016/j.envpol.2018.02.013
5. Cooper, M. J., Lamberti, G. A., Moerke, A. H., Ruetz, C. R., Wilcox, D. A., Brady, V. J., Brown, T. N., Ciborowski, J. J. H., Gathman, J. P., Grabas, G. P., Johnson, L. B., & Uzarski, D. G. (2018). An expanded fish-based index of biotic integrity for Great Lakes coastal wetlands. *Environmental Monitoring and Assessment*, *190*, 580. https://doi.org/10.1007/s10661-018-6950-6
6. Dimitriadis, P., Tegos, A., Oikonomou, A., Pagana, V., Koukouvinos, A., Mamassis, N., & Efstratiadis, A. (2016). Comparative evaluation of 1D and quasi-2D hydraulic models based on benchmark and real-world applications for uncertainty assessment in flood mapping. *Journal of Hydrology*. https://doi.org/10.1016/j.jhydrol.2016.01.020
7. Dunlop, E. S., Feiner, Z. S., & Höök, T. O. (2018). Potential for fisheries-induced evolution in the Laurentian Great Lakes. *Journal of Great Lakes Research*, *44*, 735–747. https://doi.org/10.1016/j.jglr.2018.05.009
8. Dunlop, E. S., McLaughlin, R., Adams, J. V., Jones, M., Birceanu, O., Christie, M. R., Criger, L. A., Hinderer, J. L. M., Hollingworth, R. M., Johnson, N. S., Lantz, S. R., Li, W., Miller, J., Morrison, B. J., Mota-Sanchez, D., Muir, A., Sepúlveda, M. S., Steeves, T., Walter, L., Westman, E., Wirgin, I., & Wilkie, M. P. (2017). Rapid evolution meets invasive species control: the potential for pesticide resistance in sea lamprey. *Canadian Journal of Fisheries and Aquatic Sciences*, *75*, 152–168. https://doi.org/10.1139/cjfas-2017-0015
9. Le Moal, M., Gascuel-Odoux, C., Ménesguen, A., Souchon, Y., Étrillard, C., Levain, A., Moatar, F., Pannard, A., Souchu, P., Lefebvre, A., & Pinay, G. (2019). Eutrophication: A new wine in an old bottle? *Science of The Total Environment*, *651*, 1–11. https://doi.org/10.1016/j.scitotenv.2018.09.139.
10. Mandal, S. P., & Choudhury, C. A. (2016). Flash flood risk assessment for upper Teesta river basin: using the hydrological modeling system (HEC-HMS) software. *Model Earth System and Environment*, *2*(2), 1–10. https://doi.org/10.1007/s40808-016-0110-1
11. McGoldrick, D. J., & Murphy, E. W. (2016). Concentration and distribution of contaminants in lake trout and walleye from the Laurentian Great Lakes (2008–2012). *Environmental Pollution*, *217*, 85–96. https://doi.org/10.1016/j.envpol.2015.12.019
12. Munawar, H. S., Hammad, A. W. A., & Waller, S. T. (2022). Remote Sensing Methods for Flood Prediction: A Review. *Sensors (Basel)*, *22*(3), 960. https://doi.org/10.3390/s22030960
13. Moriasi, D. N., Gitau, M. W., Pai, N., & Daggupati, P. (2015). Hydrologic and water quality models: Performance measures and evaluation criteria. *Transactions of the ASABE*, *58*(6), 1763–1785. https://doi.org/10.13031/trans.58.10715

14. Neal, J. C., Shustikova, I., Domeneghetti, A., Bates, P., & Castellarin, A. (2019). Comparing 2D capabilities of HEC-RAS and LISFLOOD-FP on complex topography. *Hydrological Sciences Journal*, *64*(14), 1769–1782. https://doi.org/10.1080/02626667.2019.1671982

15. Rabotovao, D. S., Ratsimbazafy, A. P., Andriazafimahazo, F., Rajaonah, R., Razafindrazanakolona, A. D., & Robijaona, R. B. (2025). Evaluation of Remote Sensing Data for the Identification of Lake-Stream Behavior during Normal and Cyclonic Seasons: The Case of Lake Alaotra, Madagascar. *BIAR Journal*. https://www.biarjournal.com/index.php/bioex/article/view/1310

16. Rajeshkumar, S., & Li, X. (2018). Bioaccumulation of heavy metals in fish species from the Meiliang Bay, Taihu Lake. China. *Toxicology Reports*, *5*, 288–295. https://doi.org/10.1016/j.toxrep.2018.01.007

17. Roget, E., & Khan, V. M. (2018). Decadal differences of the diurnal temperature range in the Aral Sea region at the turn of the century. *Tellus A: Dynamic Meteorology and Oceanography*, *70*, 1–12. https://doi.org/10.1080/16000870.2018.1513290

18. Sharma, S., & Lamichhane, N. (2020). Evaluation of one-dimensional and two-dimensional HEC-RAS models to predict flood travel time and inundation area for flood warning system. *ISH Journal of Hydraulic Engineering*, *28*(1), 110–126. https://doi.org/10.1080/09715010.2020.1824621

19. Sylvain Biancamaria, M., Mballo, P. Le Moigne, J. M. Sanchez Perez, G. Espitalier-Noel, Y. Grusson, R. Cakir, V. Hafliger, F. Barathieu, M. Trasmonte, A. Boone, E. Martin, & S. Sauvage. (2019). Total water storage variability from GRACE mission and hydrological models for a 50,000 km^2 temperate watershed: the Garonne River basin (France). *Journal of Hydrology: Regional Studies*, *24*. https://doi.org/10.1016/j.ejrh.2019.100609

20. Tammeorg, O., Möls, T., Niemistö, J., Holmroos, H., & Horppila, J. (2017). The actual role of oxygen deficit in the linkage of the water quality and benthic phosphorus release: Potential implications for lake restoration. *Science of The Total Environment*, *599–600*, 732–738. https://doi.org/10.1016/j.scitotenv.2017.04.244

21. Teng, J., Jakeman, A. J., Vaze, J., Croke, B. F. W., Dutta, D., & Kim, S. (2017). Flood inundation modelling: A review of methods, recent advances and uncertainty analysis. *Environmental Modelling & Software*. https://doi.org/10.1016/j.envsoft.2017.01.006

22. Teuling, A., Taylor, C., Meirink, J. F., Melsen, L., Miralles, D., van Heerwaarden, C., Vautard, R., Stegehuis, A., Nabuurs, G.-J., & Arellano, J. (2017). Observational evidence for cloud cover enhancement over western european forests. *Nature Communications*, *8*, 14065. https://doi.org/10.1038/ncomms14065.

23. Uusitalo, L., Lehikoinen, A., Helle, I., & Myrberg, K. (2015). An overview of methods to evaluate uncertainty of deterministic models in decision support. *Environmental Modelling & Software*, *63*, 24–31. https://doi.org/10.1016/j.envsoft.2014.09.017

24. Van Hyfte, S., Le Moigne, P., Bazile, E., Verrelle, A., & Boone, A. (2023). High-resolution reanalysis of daily precipitation using arome model over france. *Tellus A: Dynamic Meteorology and Oceanography*. https://doi.org/10.16993/tellusa.95

25. Yi Hong, Li, C., Lemaire, B. J., Soulignac, F., Martins, J. R. S., Roguet, A., Lucas, F., & Vincon-Leite, B. (2018). An integrated approach for assessing the impact of urban stormwater discharge on the fecal contamination in a recreational lake near Paris. In *11th International Conference on Urban Drainage Modelling*. Palermo, Italy. https://doi.org/10.1007/978-3-319-99867-1

26. Yuen, K. W., Hanh, T. T., Quynh, V. D., Switzer, A. D., Teng, P., & Lee, J. S. H. (2021). Interacting effects of land-use change and natural hazards on rice agriculture in the Mekong and Red River deltas in Vietnam. *Natural Hazards and Earth System Sciences*, *21*(5). https://doi.org/10.5194/nhess-21-1473-2021

27. Zeiger, S. J., & Hubbart, J. A. (2021). Measuring and modeling event-based environmental flows: An assessment of HEC-RAS 2D rain-on-grid simulations. *Journal of Environmental Management*, *285*, 112125. https://doi.org/10.1016/j.jenvman.2021.112125